# Self-Limiting Lithiation in Silicon Nanowires

Xiao Hua Liu,[†,*] Feifei Fan,[‡] Hui Yang,[§] Sulin Zhang,[§] Jian Yu Huang,[†,*] and Ting Zhu[‡,*]

[†]Center for Integrated Nanotechnologies (CINT), Sandia National Laboratories, Albuquerque, New Mexico 87185, United States, [‡]Woodruff School of Mechanical Engineering, Georgia Institute of Technology, Atlanta, Georgia 30332, United States, and [§]Department of Engineering Science and Mechanics, Pennsylvania State University, University Park, Pennsylvania 16802, United States

**ABSTRACT** The rates of charging and discharging in lithium-ion batteries (LIBs) are critically controlled by the kinetics of Li insertion and extraction in solid-state electrodes. Silicon is being intensively studied as a high-capacity anode material for LIBs. However, the kinetics of Li reaction and diffusion in Si remain unclear. Here we report a combined experimental and theoretical study of the lithiation kinetics in individual Si nanowires. By using *in situ*



transmission electron microscopy, we measure the rate of growth of a surface layer of amorphous $Li_xSi$ in crystalline Si nanowires during the first lithiation. The results show the self-limiting lithiation, which is attributed to the retardation effect of the lithiation-induced stress. Our work provides a direct measurement of the nanoscale growth kinetics in lithiated Si, and has implications on nanostructures for achieving the high capacity and high rate in the development of high performance LIBs.
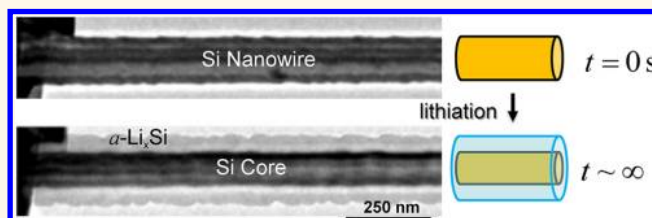
**KEYWORDS:** silicon nanowire · lithium-ion battery · kinetics · self-limiting lithiation · stress retardation · *in situ* transmission electron microscopy

Lithium-ion batteries (LIBs) are critically important for electrifying transport vehicles and delivering renewable electricity.[1] Future competitive applications of LIBs are hinged on the ability to drastically improve the capacity, rate, and cycle life. These requirements are crucially controlled by the kinetics of Li reaction and diffusion in solid-state electrodes.[2–4] To enable the drastic performance improvement of LIBs, it is imperative to characterize, understand, and optimize the Li kinetics in electrodes.[5–8]

Experiments show that Li insertion into the high-capacity anode material, such as Si nanowires and nanoparticles, occurs through the growth of an amorphous alloy of $Li_xSi$ (denoted as $a$-$Li_xSi$, where $x \approx 3.75$).[8–12] Such a Li-rich amorphous product is separated from the unreacted crystalline Si ($c$-Si) by an atomically sharp phase boundary. During progressive lithiation, the Li is supplied from the nanowire/nanoparticle surface and must diffuse across the $a$-$Li_xSi$ layer that grows with increasing thickness. While the lithiation processes have been studied by various experimental techniques,[8–17] the kinetics of lithiation in Si nanomaterials remain unclear. From both the experimental[8–17] and

modeling[18–29] standpoints, there is currently a strong need to quantify the lithiation kinetics in Si. This is central for advancing the understanding and development of high-capacity Si-based anodes.

Recently, McDowell et al.[17] studied the lithiation kinetics in $c$-Si nanoparticles with different initial diameters using *in situ* transmission electron microscopy (TEM). They measured the positions of the reaction front (*i.e.*, the phase boundary between the $c$-Si core and $a$-$Li_xSi$ shell) during lithiation, and attributed the slowing of the reaction front to the changing mechanical stress at the reaction front that altered the driving force for reaction. This work raises a series of fundamental questions. For example, is the slowing of the lithiation rate primarily caused by the stress retardation effect on the Li reaction at the phase boundary or Li diffusion in the lithiated $a$-$Li_xSi$ layer? How is the slowing of the lithiation rate affected by the curved phase boundary and the applied voltage? What is the size effect of nanoparticles/nanowires on the lithiation rate? To shed light onto these questions, here we report a combined experimental and theoretical study of growth kinetics of $a$-$Li_xSi$ in a

c-Si nanowire during the first lithiation. Taking advantage of the large contrast in electron transparency between the crystalline and amorphous phases, the real-time imaging through TEM allows a direct measurement of the growth rate of $a$-Li$_x$Si at the nanoscale. Our *in situ* TEM results not only provide the quantitative data of lithiation kinetics in Si nanowires, but also reveal the self-limiting behavior of lithiation, which is attributed to the stress-retardation effect. This work represents a significant step toward deconvoluting the composition, geometry, and stress effects on the lithiation kinetics in Si alloys, essential to the development of high-rate and high-capacity electrodes for LIBs.

## RESULTS AND DISCUSSION

Figure 1a,b shows a schematic illustration of the *in situ* lithiation experiment inside the TEM. A nanobattery was constructed in the half-cell configuration using the Si nanowire (SiNW) working electrode, as described elsewhere.[9,30] As indicated in Figure 1b, after a bias of −2 V was applied to the SiNWs, Li transport took place through all free surfaces (*i.e.*, on Si wafer and adjacent SiNWs, marked by the red arrows), and lithiation occurred from the surfaces into the bulk of *c*-Si. Figure 1c shows a pristine SiNW, while Figure 1d shows the partially lithiated SiNW with an $a$-Li$_x$Si shell grown on the inner *c*-Si core. The interface between the $a$-Li$_x$Si shell and *c*-Si core was sharp, indicating the two-phase mechanism of Li insertion into Si. Figure 1e shows a low-magnification TEM image of the multiple SiNWs being lithiated, and the red arrows mark the surface diffusion path of Li. Notably, lithiation also occurred in those SiNWs that were not directly contacting the Li$_2$O/Li electrodes. The inset in Figure 1e illustrates Li transport on the surface, as well as radial insertion into the *c*-Si core.

The growth kinetics of the $a$-Li$_x$Si shell on *c*-Si was obtained by monitoring the SiNW morphology in every 15 min. All the experiments were conducted without the electron beam illumination (*i.e.*, in dark) except for quick imaging at the weak beam (electron dosage rate of ∼2.5 mA/cm$^2$). To reveal the intrinsic lithiation behavior without the influence of externally applied voltage and force, we chose to monitor a freestanding SiNW, the bottom image in Figure 1e, denoted as SiNW_A. Figure 2a−e shows the evolution of the morphology and two-phase microstructure in SiNW_A. In Figure 2f, we plot the thickness of the $a$-Li$_x$Si shell *versus* time, as well as the diameter changes of the Si core and the etched depth, taken from a typical cross section of SiNW_A. During the lithiation process over 4 h, the diameter of the *c*-Si core decreased from 139 to 101 nm, and the thickness of the $a$-Li$_x$Si grew from 0 to 54 nm. In the first hour, the lithiation was fast and the average velocity of the core−shell interface was about 10 nm per hour or equivalently $3 \times 10^{-12}$ m/s. The lithiation apparently slowed down as the core−shell interface moved deeply to the center of SiNW_A, and

became extremely slow after about 2.5 h. These results clearly demonstrate the self-limiting lithiation in Si nanomaterials.

In addition to SiNW_A, we also monitored the relatively fast lithiation of a SiNW in direct contact with the Li$_2$O/Li electrode, the top image in Figure 1e, denoted as SiNW_B. Since SiNW_B was subjected to the applied voltage, the lithiation rate was markedly increased. Figure 2g−k shows the morphological evolution of SiNW_B. Figure 2l shows the thickness of the $a$-Li$_x$Si shell *versus* time, as well as the diameter changes of the Si core and the etched depth. During the first 1.5 h of lithiation, the diameter of the *c*-Si core decreased from 129 to 58 nm, and the thickness of the $a$-Li$_x$Si grew from 0 to 95 nm. Compared to SiNW_A, the lithiation in SiNW_B was faster, and the average velocity of the core−shell interface was about 35 nm per hour or equivalently $10^{-11}$ m/s. Incidentally, this average velocity represents the mean value over a long span of an hour, and thus it is markedly lower than the initial velocity of the ⟨110⟩ interface—about $5 \times 10^{-11}$ m/s as measured by recent *in situ* high resolution TEM experiments under the same applied voltage during the early stage of lithiation.[8] Also note that in the above estimate the growth in the first half an hour was not included, because the initial lithiation rate was extremely low, possibly due to the incubation time required for formation of a percolating path of Li-ion transport through the solid electrolyte Li$_2$O or Li penetration into Si subsurface. Similar to SiNW_A, SiNW_B also exhibited the self-limiting lithiation, as the movement of the core−shell interface became extremely slow after about 1.5 h. When the lithiation was fully retarded (after 4 h in both cases), the diameter of the *c*-Si core was smaller in SiNW_B than that in SiNW_A, indicating the varying extent of lithiation by the applied voltage. The Supporting Information movie shows the lithiation process of both SiNWs in the same field of view. The slowing of the lithiation front was also recently observed in Si nanoparticles by McDowell *et al.*[17] Their lithiation time scale is on the order of minutes, as opposed to hours in our experiment. The large difference in time scale is possibly due to the different conditions of applied voltage and doping in Si, *etc.*, but indicative of the robustness of the self-limiting lithiation behavior.

As this work primarily focuses on the intrinsic chemical lithiation behavior of Si nanomaterials, we will further analyze the lithiation kinetics in SiNW_A. This has been facilitated by the large set of collected data that clearly reveal the time law of growth. Before embarking upon detailed analyses of the lithiation kinetics, we outline a general theory of solid-state reactions involving the moving phase boundaries (with detailed derivation given in the Supporting Information).[31,32] To highlight the essential physics, we first consider a simplified geometry where a planar film of $a$-Li$_x$Si ($\gamma$ phase) grows between the pure phases of Li ($\alpha$) and Si ($\beta$), as shown in Figure 3a.
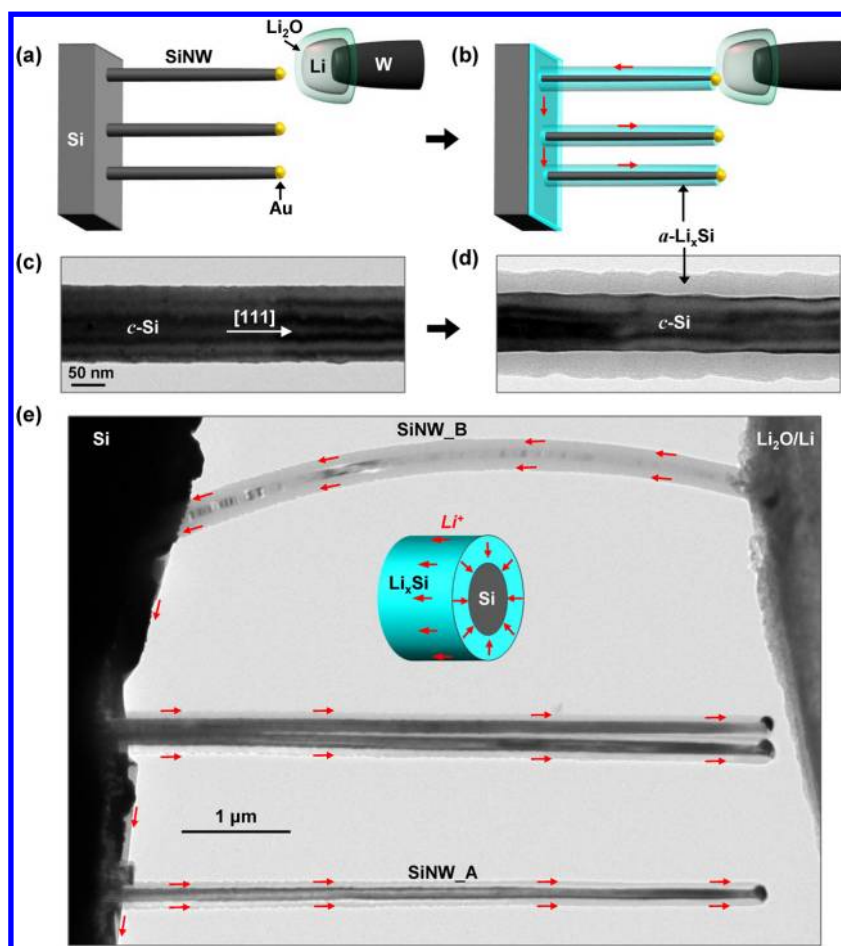
**Figure 1.** *In situ* lithiation of SiNWs. (a,b) Schematic illustration of the experimental setup. The [111]-oriented SiNWs were epitaxially grown on a Si(111) wafer, and the $Li_2O$/Li electrode on a W probe was brought to contact the free end of a SiNW. Upon lithiation, Li diffused on all the surfaces and lithiation occurred also on adjacent freestanding SiNWs. (c,d) Morphology comparison between the pristine (c) and lithiated SiNW (d). An *a*-$Li_x$Si shell was growing on the *c*-Si core during lithiation. (e) An overall view of several SiNWs being lithiated. The inset scheme shows Li diffusion on the NW surface and radial insertion. The freestanding SiNW marked as SiNW_A was lithiated by the Li flux coming from SiNW_B that was in contact with $Li_2O$/Li.

The growth kinetics of the *a*-$Li_x$Si alloy layer is determined by two types of processes in series: (1) the *diffusion* of Li across the alloy layer with increasing thickness; (2) the reaction at the interface that usually involves a reaction barrier. Figure 3b shows that in the diffusion-controlled limit, the Li concentration at the interfaces is given by the equilibrium values of $C_{\gamma\alpha}^{eq}$ and $C_{\gamma\beta}^{eq}$, defined in terms of the common tangent of the free energy curves, as schematically shown in Figure 3c. The corresponding rate-controlling parameter is the interdiffusion coefficient $D$ in the lithiated alloy—since the mobility of Li is usually much higher than that of Si,[26] $D$ can be reasonably regarded as the Li diffusivity. Figure 3b also shows that in the reaction-controlled limit, the actual concentrations at the interfaces are $C_{\gamma\alpha} < C_{\gamma\alpha}^{eq}$ and $C_{\gamma\beta} > C_{\gamma\beta}^{eq}$, respectively. The associated rate-controlling parameter is the interfacial reaction rate constants of $\kappa_{\gamma\alpha}$ and $\kappa_{\gamma\beta}$. Between the two limits, the rate of change of the layer thickness, $X_\gamma = X_{\gamma\beta} - X_{\alpha\gamma}$, is given by

$$\frac{dX_\gamma}{dt} = \frac{(C_{\gamma\alpha}^{eq} - C_{\gamma\beta}^{eq})\kappa_\gamma H_\gamma}{1 + \frac{\kappa_\gamma X_\gamma}{D}} \quad (1)$$

where the effective interfacial reaction constant $\kappa_\gamma$ is $1/\kappa_\gamma = 1/\kappa_{\gamma\alpha} + 1/\kappa_{\gamma\beta}$ and the growth coefficient $H_\gamma$ is $H_\gamma = 1/(C_{\alpha\gamma}^{eq} - C_{\gamma\alpha}) + 1/(C_{\gamma\beta} - C_{\beta\gamma}^{eq})$.

Equation 1 reveals the key dimensionless parameter, $\kappa_\gamma X_\gamma/D$, that governs the aforementioned reaction- and diffusion-controlled limits. Namely, when $\kappa_\gamma X_\gamma/D \ll 1$, the interface reaction dominantly controls the growth rate. Correspondingly, eq 1 is reduced to

$$\frac{dX_\gamma}{dt} = M^i \quad (2)$$

where $M^i = (C_{\gamma\alpha}^{eq} - C_{\gamma\beta}^{eq})\kappa_\gamma H_\gamma$. Integration of eq 2 gives the thickness $X_\gamma$ proportional to $t$, called the linear growth. When $\kappa_\gamma X_\gamma/D \gg 1$, this is the regime of diffusion-controlled growth. It follows that eq 1 is reduced to

$$\frac{dX_\gamma}{dt} = \frac{M^d}{X_\gamma} \quad (3)$$

where $M^d = D(C_{\gamma\alpha}^{eq} - C_{\gamma\beta}^{eq})H_\gamma$ and $H_\gamma = 1/(C_{\alpha\gamma}^{eq} - C_{\gamma\alpha}^{eq}) + 1/(C_{\gamma\beta}^{eq} - C_{\beta\gamma}^{eq})$. Integration of eq 3 yields the thickness $X_\gamma$ proportional to $\sqrt{t}$, called the parabolic growth. It should
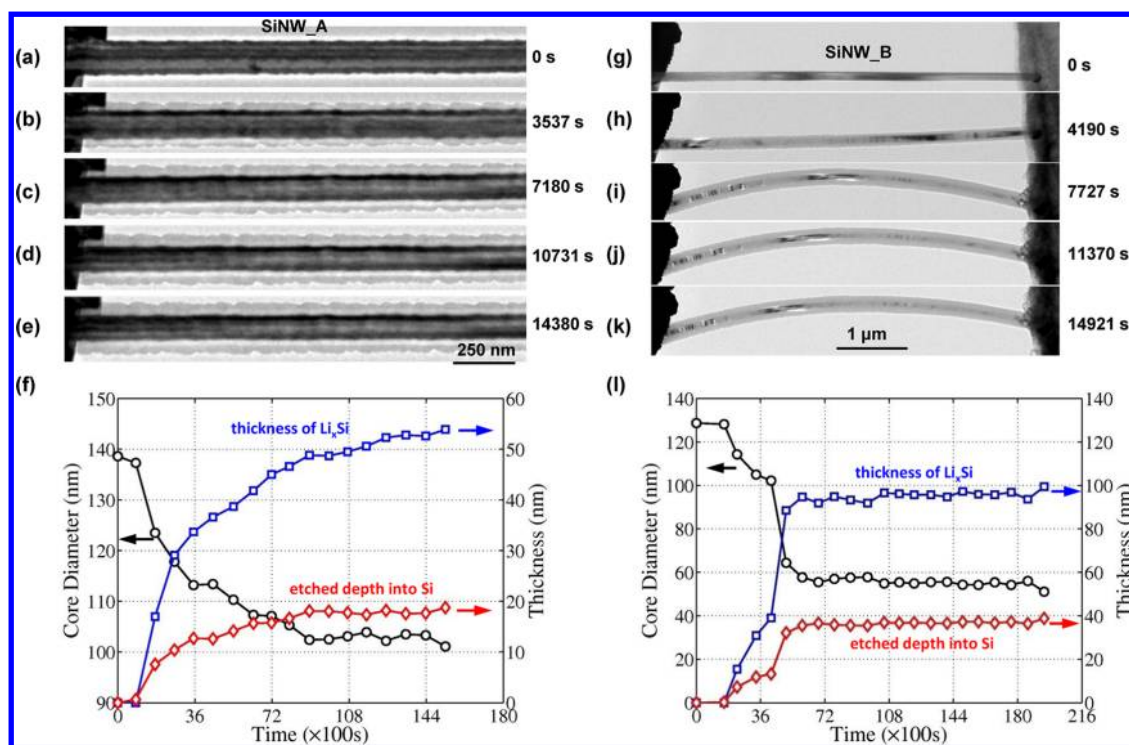
**Figure 2.** Growth kinetics of amorphous Li—Si alloy on SiNWs. (a—e) Morphological evolution of SiNW_A in 4 h. (f) Plots of etch depth and diameter of SiNW_A and thickness of the $a$-Li$_x$Si shell *versus* time. (g—k) Morphological evolution of SiNW_B in 4 h. (l) Lithiation kinetics of SiNW_B. The growth of $a$-Li$_x$Si slowed down in both SiNW_A and B during the long lithiation process.
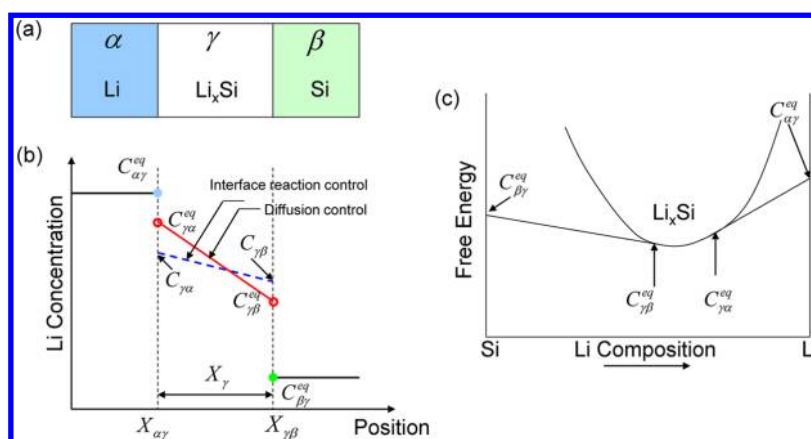


**Figure 3.** Free energy and concentration profile governing the growth of an amorphous Li$_x$Si layer, adapted from Gosele and Tu.[31,32] (a) The product phase of Li$_x$Si ($\gamma$) grows in between the parent phases of Li ($\alpha$) and Si ($\beta$). (b) Li concentration profile through the thickness of the multilayer, showing the limits of the interface reaction control and the diffusion control. The equilibrium Li concentration in $\alpha$ and $\beta$ phase is denoted by $C_{\alpha\gamma}^{eq}$ and $C_{\beta\gamma}^{eq}$, respectively; within the layer of $\gamma$ phase, the equilibrium concentrations at the $\gamma$—$\beta$ and $\gamma$—$\alpha$ interface are denoted as $C_{\gamma\alpha}^{eq}$ and $C_{\gamma\beta}^{eq}$, respectively. These concentrations can be determined by the common-tangent method in the plot of free energy as a function of Li concentration, as schematically shown in panel c.

be noted that for conceptual clarity the above variables are all defined in terms of the reference state of pure Si, as opposed to the current lithiated state. For example, the Li concentration is the number of Li per reference volume in pristine Si, and $X_\gamma$ is the thickness of the pristine Si layer that has been lithiated. In our experiments, the initial radius of SiNW, $B$, the current radius of lithiated SiNW, $b$, and the current radius of Si core, $A$, were all directly measured. As a result, one can study the time-dependent

thickness of the lithiated Si shell either in the reference state (*i.e.*, the pristine Si shell that has been lithiated, $X_\gamma = B - A$) or in the current state (*i.e.*, the $a$-Li$_{3.75}$Si shell, $x_\gamma = b - A$). Formulation in terms of the reference state is often adopted in continuum mechanics for problems with large deformation. Such an approach avoids the complication on Li flux arising from volume expansion. The following analyses will be performed on the basis of the reference state. However, given the one-to-one correspondence

between $X_\gamma$ and $x_\gamma$ measured in experiments, the final results will be presented in terms of the current thickness, which is more intuitive.

Next, we apply the above theory to analyze the measured lithiation kinetics in SiNW_A. Recall that lithiation occurs through the core−shell mode, that is, a shell of $a$-Li$_x$Si grows with concomitant shrinkage of a $c$-Si core. Figure 1e reveals that the tapering of the Si core is negligibly small in the longitudinal direction, suggestive of considerably faster Li diffusion on the surface than in the bulk. On this basis one can focus on the radial lithiation within a representative cross section of SiNW_A by taking the surface Li concentration as a boundary condition. As such, the 3D lithiation problem is reduced to 2D. Moreover, recent experiments have revealed the anisotropic swelling in $c$-Si nanowires and microslabs upon lithiation, with the largest expansion in the ⟨110⟩ direction.[9−11] However, for a ⟨111⟩-orientated SiNW, there is a high number of (i.e., six) equivalent ⟨110⟩ directions within the cross section, such that the isotropic lithiation in the nanowire cross section can be reasonably assumed. Hence the 2D analysis is further reduced to 1D in the radial direction. As such, the following analyses of lithiation kinetics should be considered as those related to ⟨110⟩ interfaces.

It should be stressed that the rate of growth of the $a$-Li$_x$Si shell (as given by the slope of the blue curve in Figure 2f) is not constant in SiNW_A. The origin of such nonlinear growth cannot be clearly determined at the moment of this study. This is because the lithiation-induced compressive stresses in the $a$-Li$_x$Si layer could dominantly retard either the Li diffusion in the shell or the Li reaction at the core−shell interface. To shed light on the stress-lithiation coupling, we consider both the limits of diffusion- and reaction-control, respectively. First, we assume that the growth kinetics are controlled by Li diffusion. Taking the Li concentration at the nanowire surface, $C_s$, as a prescribed boundary condition, we reduce the rate coefficient $M^d$ in eq 3 to

$$M^d = D \frac{C_s - C^{eq}_{\gamma\beta}}{C^{eq}_{\gamma\beta} - C^{eq}_{\beta\gamma}} \tag{4}$$

Numerical integration of eqs 3 and 4 yields the time law of growth, that is, thickness of the lithiated layer as a function of time, when the phase boundary is planar.

To account for the self-limiting behavior of lithiation in SiNWs, we note that the core−shell interface is curved. Our analysis indicates that the self-limiting of lithiation cannot be simply explained by a geometrical curvature effect, which leads to the increased circumferential length with radial distance. This is shown in Figure 4b by the large discrepancy between the experimental data and the modeling result (green dashed line) from direct numerical integration of eqs 3 and 4 with the geometrical curvature effect incorporated. Apparently, the measured data are highly nonlinear and deviate from the classic linear or parabolic relation.[31−33] We attribute the discrepancy between experiment and modeling to the stress retardation effect that will be accounted for in eqs 3 and 4, rather than inadequate parameter optimization.

To rationalize the slowing of the reaction front, we note that the large compressive stresses can develop in the lithiated shell, owing to geometrical constraints from the unlithiated $c$-Si core. At this moment, the stress evolution in lithiated Si cannot be quantitatively evaluated, due to a lack of experimentally measured chemo-mechanical properties of Li$_x$Si such as chemical strains of Li insertion and elasto-plastic properties, all of which depend sensitively on Li concentration and possibly on crystal orientation.[34,35] Nevertheless, we employ a chemo-mechanical model, as described in detail in our recent work,[9,20,36] to qualitatively capture the dominant feature of lithiation-induced stresses in SiNWs when the two-phase mechanism of lithiation is involved. In Figure 4a, we plot the representative results of lithiation-induced stresses, showing the large hydrostatic compression generated in the lithiated shell.

To evaluate the impact of the lithiation-induced compressive stresses, we assume, in a first approximation, a uniform hydrostatic compression $p$ within the lithiated shell. Then the effective diffusivity can be expressed as $D = D_0 \exp(-p\Omega/k_BT)$, where $D_0$ is the Li diffusivity at zero stress, $\Omega$ is the activation volume of Li diffusion, and $k_BT$ is the thermal energy. As shown in Figure 4a, the uniform pressure $p$ represents a reasonable approximation, when the lithiated shell is thin. However, the pressure $p$ can become highly nonuniform as the reaction front further moves to the center of SiNW. This has been recently shown to be caused by the increasing importance of the curvature effect of the reaction front, i.e., the lithiation-induced volume expansion at the curved reaction front pushes out materials in the lithiated shell, leading to the reversal of hoop stress from the initial compression to tension in the shell.[12,37] In SiNW_A, the slowing of the reaction front occurs when the lithiated shell is thin, such that the use of a uniform $p$ is reasonably justified. Furthermore, during the early stage of lithiation, the pressure $p$ increases as the lithiated shell thickens.[12,20,36] This arises similarly owing to the effect of the curved reaction front, namely, the lithiation-induced pressure at the reaction front has to increase in order to push out the materials in the thickening shell. To account for the effect of increasing pressure in the lithiated shell, we rewrite the above stress-dependent Li diffusivity as

$$D = D_0 \exp[-(\alpha X_r/B)^\beta] \tag{5}$$

where $B$ denotes the initial radius of SiNW and is introduced to normalize $X_r$. In eq 5, $\alpha$ and $\beta$ are the dimensionless fitting parameters. This empirical formula involves a stretched exponential function, giving
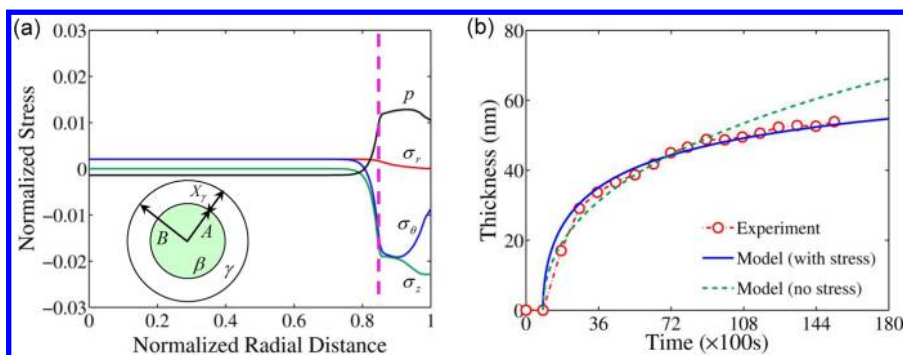
**Figure 4. Modeling of stress generation and self-limiting lithiation in a SiNW. (a)** Computed radial stress distribution at the cross section, including the radial $\sigma_r$, hoop $\sigma_\theta$, axial $\sigma_z$, and hydrostatic compression $p = -(\sigma_r + \sigma_\theta + \sigma_z)/3$ components, which are normalized by Young's modulus. The radial distance is normalized by the cross-sectional radius of SiNW. The dashed line indicates the current location of the core−shell interface. The inset shows the schematic of the cross section of a partially lithiated SiNW, where an $a$-Li$_x$Si shell encloses a $c$-Si core. **(b)** Thickness of the $a$-Li$_x$Si shell *versus* time: comparison between experiment (circles) and modeling that includes the stress-retardation effect (blue line); also shown is the fitting curve (green dashed line) from the stress-free model where the stress-independent diffusivity is optimized to improve the overall quality of fitting.

the effective diffusivity that decreases with increasing shell thickness. As shown in Figure 4b, the modeling result can well match the experimentally measured values of $X_r$ as a function of time. The fitting parameters are $\alpha = 5$ and $\beta = 2$; the detailed fitting formulas and numerical procedures are given in the Supporting Information. The effectiveness of eq 5 suggests a strong nonlinear influence of lithiation-induced stresses on the lithiation kinetics, while the linear stress effect has been usually assumed in previous models of stress-diffusion coupling for Si electrodes. In addition, we obtain the fitting value of $D_0 \approx 10^{-13}$ cm$^2$/s, corresponding to the Li diffusivity in $a$-Li$_{3.75}$Si at zero stress and room temperature. However, this diffusivity is extracted indirectly and should be considered as an estimate. Moreover, the Si substrate also absorbs Li, thus affecting the Li concentrations at the surface of SiNW_A and accordingly the driving force of Li diffusion into the bulk of SiNW_A. These effects cannot be quantitatively evaluated at this moment. Nevertheless, our estimated diffusivity is reasonably close to the reported experimental values in the literature (in the range of $10^{-13}$ to $10^{-12}$ cm$^2$/s),[14,38] considering that various factors such as doping could change the lithiation rate.[39]

Although the self-limiting lithiation might be caused by the stress-retarded diffusion owing to the high compressive stresses generated in the lithiated shell, the present experimental results cannot exclude the possible cause of self-limiting lithiation by the stress-retarded interface reaction. To evaluate the interface-reaction limit, we assume that the Li reaction at the nanowire surface is faster than in the bulk, and thus take the surface Li concentration of SiNW, $C_s$, as a prescribed boundary condition. It follows that the rate coefficient $M^i$ in eq 2 becomes

$$M^i = \frac{C_s - C_{\gamma\beta}^{eq}}{C_s - C_{\beta\gamma}^{eq}} \kappa_{\gamma\beta} \qquad (6)$$

where the Li concentration $C_{\gamma\beta}$ at the core−shell interface has been approximated by $C_s$. Similar to the above diffusion-limited case, we adopt an empirical function to represent the nonlinear effect of lithiation-induced pressure at the core−shell interface, that is, $\kappa_{\gamma\beta} = \kappa_{\gamma\beta 0}$ $\exp[-(\alpha X_r/B)^\beta]$, where $\kappa_{\gamma\beta 0}$ denotes the rate constant at the reaction front at zero stress; this relation physically reflects the fact that the pressure at the core−shell interface increases as the shell grows thicker, thus increasing the activation energy barrier and accordingly lowering the reaction rate. In the Supporting Information, Figure S2 shows that the modeling result well matches the experimentally measured values of $X_r$ as a function of time. The fitting parameters are $\kappa_{\gamma\beta 0} = 5 \times 10^{-10}$ m/s, $\alpha = 6$ and $\beta = 2$. In addition, we note that the lithiation-induced stress generally affects both the thermodynamics (*e.g.*, diffusion potential) and kinetics (*e.g.*, energy barrier) of diffusion/reaction simultaneously.[21] In the above analyses of diffusion/reaction control, we adopt the Arrhenius rate relation to account for the stress retardation effect. This approach allows us to directly fit the measured data of lithiation kinetics and also renders a strong nonlinear influence of stress on lithiation. In the future, it is interesting to study the relationship between such a kinetic approach and the thermodynamic analysis in terms of the stress-retarded diffusion/reaction potential.

To understand the size effect on lithiation kinetics and particularly on the self-limiting feature, we note that McDowell *et al.*[17] studied the lithiation kinetics in crystalline Si nanoparticles with different initial radii $B$. They showed that the slowing of the reaction front depends primarily on the ratio of $X_r/B$. In other words, it is not dependent on the nanoparticle size after appropriate rescaling of the measured data. Motivated by their work, we derive a scaling relation in the Supporting Information, which reveals how the lithiation kinetics vary with the nanowire/nanoparticle radius. Specifically, we show that the ratio of $X_r/B$ should obey

a size-independent time law under reaction control, and a scaling relation can be similarly derived in the case of diffusion control. These results suggest that the self-limiting feature should not depend on the wire/particle size, as long as the mechanical stress scales with the dimensionless variable of $X_r/B$, a condition that is satisfied when the classic elasto-plastic deformation (which is length scale independent) prevails. As a consequence of such size independence, it remains an open question regarding how to determine the rate-controlling step for the stress-mediated lithiation that deviates from the classic linear or parabolic relation.[31−33]

Finally, we note that for several other free-standing SiNWs in Figure 1e, we obtained the similar kinetics data as for SiNW_A. However, SiNW_B was in direct contact with the Li source and subjected to the applied voltage. As a result, its electrochemical lithiation involves a more complicated coupling between the electron/ion transport with the electric and stress fields. Figure 2l shows that the position of the reaction front appears to depend linearly on time, suggestive of the interface-reaction control. However, in this case the reaction front moves deeply to the center of the nanowire and the stress distribution in the lithiated shell becomes highly nonuniform, so that the assumption of the uniform shell stress is not valid.[12] In addition, due to the uncertainty on the contact resistance between the $Li_2O$/Li electrode and SiNW_B, the voltage acting on SiNW_B is not quantitatively known. Furthermore, the analysis of the electrochemical lithiation in SiNW_B, as opposed to the chemical lithiation in SiNW_A without the applied voltage, requires the quantitative information about the effects of electrical field on both Li diffusion and interface reaction, which is not available at the moment of this study. But the self-limited electrochemical lithiation in cases such as SiNW_B is an important problem that requires a systematic study in the future.

The result of self-limiting lithiation has implications for achieving the high capacity and high rate in the development of Si-based anodes for high-performance LIBs. First, the hollow nanotubes should be more favorably used as the anode materials than the solid nanowires. The experiments show that the velocity of the reaction front is drastically reduced as it moves to the center of the nanowire. As a result of the slowing of the lithiation reaction (which is retarded by the lithiation

stress), it would be difficult to fully lithiate all the solid Si nanowires. During *in situ* lithiation experiments, we frequently observed the unlithiated core that could not be further lithiated, such that the effective Li capacity in the Si nanowires is reduced. Since the stress-retardation effect on lithiation kinetics arises from the curved core−shell interface, the above considerations are also applicable to Si nanoparticles. Both the hollow Si nanowires and nanoparticles have been previously studied, but mostly from the perspective of mitigating the mechanical degradation[40−42] rather than from the capacity and rate considerations. Our work of self-limiting lithiation provides a new perspective.

Second, the self-limiting behavior of lithiation is encouraged by the two-phase lithiation mechanism in *c*-Si nanowires during the first lithiation. The large and abrupt change of Li concentration across the phase boundary (that is, core−shell interface) facilitates the buildup of high compressive stresses in the lithiated shell, thereby causing the slow-down of Li diffusion and interface reaction. In this regard, a natural question is what happens beyond the first lithiation of *c*-Si. Our recent *in situ* TEM experiments indicate that the two-phase lithiation mechanism prevails not only in *c*-Si but also in the first lithiation of *a*-Si. As such, the implications discussed above are expected to be applicable to *a*-Si. However, it remains an open question whether the two-phase mechanism dominates the lithiation of *a*-Si beyond the first cycle—such possibility has not been clearly proved or disapproved by the *in situ* experiment so far, but should be further studied in the future.

## CONCLUSION

In summary, we measure the rate of growth of a surface layer of amorphous $Li_xSi$ in the crystalline Si nanowire during the first lithiation by using *in situ* transmission electron microscopy. The self-limiting lithiation of Si is observed, which is attributed to the retardation effect of the lithiation-induced stress. We show that the chemical lithiation can occur spontaneously in Si nanowires, but its kinetics are much slower than the electrochemical lithiation under the applied voltage. Our work provides a direct measurement of the nanoscale lithiation kinetics in Si, as well as a mechanistic framework for quantifying the rates of high-capacity anodes in the development of high-performance lithium-ion batteries.

## EXPERIMENTAL DETAILS

The SiNWs, epitaxially grown on a Si (111) wafer, were the working electrode; the Li metal on a tungsten (W) probe was the counter electrode; and a native lithium oxide ($Li_2O$) layer acted as a solid-state electrolyte (Figure 1a). The $Li_2O$/Li electrode was driven by a piezo-positioner (Nanofactory, TEM-scanning tunneling microscopy holder) to contact the free end of a SiNW, and then a bias of −2 V was applied to the Si wafer with

respect to the W probe to initiate and sustain the lithiation. The current compliance was set at 1 nA to avoid additional disturbing effects (*i.e.*, uneven lithiation or Joule-heating). The electron beam was shut off during lithiation, except for the periodic imaging. During the imaging process, the total exposure time was about several seconds and the electron dosage rate was minimized to avoid beam effect on the reaction kinetics.

*Supporting Information Available:* The details of modeling and the supporting movie showing the self-limiting lithiation of SiNWs are provided. This material is available free of charge *via* the Internet at http://pubs.acs.org.

## REFERENCES AND NOTES

1. Tarascon, J. M.; Armand, M. Issues and Challenges Facing Rechargeable Lithium Batteries. *Nature* **2001**, *414*, 359–367.

2. Goodenough, J. B.; Kim, Y. Challenges for Rechargeable Li Batteries. *Chem. Mater.* **2010**, *22*, 587–603.

3. Li, H.; Huang, X. J.; Chen, L. Q.; Wu, Z. G.; Liang, Y. A High Capacity Nano-Si Composite Anode Material for Lithium Rechargeable Batteries. *Electrochem. Solid State Lett.* **1999**, *2*, 547–549.

4. Chan, C. K.; Peng, H. L.; Liu, G.; McIlwrath, K.; Zhang, X. F.; Huggins, R. A.; Cui, Y. High-Performance Lithium Battery Anodes Using Silicon Nanowires. *Nat. Nanotechnol.* **2008**, *3*, 31–35.

5. Huang, J. Y.; Zhong, L.; Wang, C. M.; Sullivan, J. P.; Xu, W.; Zhang, L. Q.; Mao, S. X.; Hudak, N. S.; Liu, X. H.; Subramanian, A.; *et al. In Situ* Observation of the Electrochemical Lithiation of a Single SnO₂ Nanowire Electrode. *Science* **2010**, *330*, 1515–1520.

6. Chiang, Y. M. Building a Better Battery. *Science* **2010**, *330*, 1485–1486.

7. Weichert, K.; Sigle, W.; van Aken, P. A.; Jamnik, J.; Zhu, C. B.; Amin, R.; Acarturk, T.; Starke, U.; Maier, J. Phase Boundary Propagation in Large LiFePO₄ Single Crystals on Delithiation. *J. Am. Chem. Soc.* **2012**, *134*, 2988–2992.

8. Liu, X. H.; Wang, J. W.; Huang, S.; Fan, F.; Huang, X.; Liu, Y.; Krylyuk, S.; Yoo, J.; Dayeh, S. A.; Davydov, A. V.; *et al. In Situ* Atomic-Scale Imaging of Electrochemical Lithiation in Silicon. *Nat. Nanotechnol.* **2012**, *7*, 749–756.

9. Liu, X. H.; Zheng, H.; Zhong, L.; Huang, S.; Karki, K.; Zhang, L. Q.; Liu, Y.; Kushima, A.; Liang, W. T.; Wang, J. W.; *et al.* Anisotropic Swelling and Fracture of Silicon Nanowires During Lithiation. *Nano Lett.* **2011**, *11*, 3312–3318.

10. Goldman, J. L.; Long, B. R.; Gewirth, A. A.; Nuzzo, R. G. Strain Anisotropies and Self-Limiting Capacities in Single-Crystalline 3D Silicon Microstructures: Models for High Energy Density Lithium-Ion Battery Anodes. *Adv. Funct. Mater.* **2011**, *21*, 2412–2422.

11. Lee, S. W.; McDowell, M. T.; Choi, J. W.; Cui, Y. Anomalous Shape Changes of Silicon Nanopillars by Electrochemical Lithiation. *Nano Lett.* **2011**, *11*, 3034–3039.

12. Liu, X. H.; Zhong, L.; Huang, S.; Mao, S. X.; Zhu, T.; Huang, J. Y. Size-Dependent Fracture of Silicon Nanoparticles During Lithiation. *ACS Nano* **2012**, *6*, 1522–1531.

13. Ruffo, R.; Hong, S. S.; Chan, C. K.; Huggins, R. A.; Cui, Y. Impedance Analysis of Silicon Nanowire Lithium Ion Battery Anodes. *J. Phys. Chem. C* **2009**, *113*, 11390–11398.

14. Pharr, M.; Zhao, K.; Wang, X.; Suo, Z.; Vlassak, J. J. Kinetics of Initial Lithiation of Crystalline Silicon Electrodes of Lithium-Ion Batteries. *Nano Lett.* **2012**, *12*, 5039–5047.

15. Gu, M.; Li, Y.; Li, X. L.; Hu, S. Y.; Zhang, X. W.; Xu, W.; Thevuthasan, S.; Baer, D. R.; Zhang, J. G.; Liu, J.; *et al. In Situ* TEM Study of Lithiation Behavior of Silicon Nanoparticles Attached to and Embedded in a Carbon Matrix. *ACS Nano* **2012**, *6*, 8439–8447.

16. Ghassemi, H.; Au, M.; Chen, N.; Heiden, P. A.; Yassar, R. S. *In Situ* Electrochemical Lithiation/Delithiation Observation of Individual Amorphous Si Nanorods. *ACS Nano* **2011**, *5*, 7805–7811.

17. McDowell, M. T.; Ryu, I.; Lee, S. W.; Wang, C.; Nix, W. D.; Cui, Y. Studying the Kinetics of Crystalline Silicon Nanoparticle Lithiation with *In Situ* Transmission Electron Microscopy. *Adv. Mater.* **2012**, *24*, 6034–6041.

18. Deshpande, R.; Cheng, Y. T.; Verbrugge, M. W.; Timmons, A. Diffusion Induced Stresses and Strain Energy in a Phase-Transforming Spherical Electrode Particle. *J. Electrochem. Soc.* **2011**, *158*, A718–A724.

19. Gao, Y. F.; Zhou, M. Strong Stress-Enhanced Diffusion in Amorphous Lithium Alloy Nanowire Electrodes. *J. Appl. Phys.* **2011**, *109*, 014310.

20. Yang, H.; Huang, S.; Huang, X.; Fan, F. F.; Liang, W. T.; Liu, X. H.; Chen, L. Q.; Huang, J. Y.; Li, J.; Zhu, T.; *et al.* Orientation-Dependent Interfacial Mobility Governs the Anisotropic Swelling in Lithiated Silicon Nanowires. *Nano Lett.* **2012**, *12*, 1953–1958.

21. Zhao, K. J.; Pharr, M.; Wan, Q.; Wang, W. L.; Kaxiras, E.; Vlassak, J. J.; Suo, Z. G. Concurrent Reaction and Plasticity During Initial Lithiation of Crystalline Silicon in Lithium-Ion Batteries. *J. Electrochem. Soc.* **2012**, *159*, A238–A243.

22. Cui, Z.; Gao, F.; Qu, J. A Finite Deformation Stress-Dependent Chemical Potential and Its Applications to Lithium Ion Batteries. *J. Mech. Phys. Solids* **2012**, *60*, 1280–1295.

23. Chevrier, V. L.; Dahn, J. R. First Principles Model of Amorphous Silicon Lithiation. *J. Electrochem. Soc.* **2009**, *156*, A454–A458.

24. Huang, S.; Zhu, T. Atomistic Mechanisms of Lithium Insertion in Amorphous Silicon. *J. Power Sources* **2011**, *196*, 3664–3668.

25. Zhao, K. J.; Wang, W. L.; Gregoire, J.; Pharr, M.; Suo, Z. G.; Vlassak, J. J.; Kaxiras, E. Lithium-Assisted Plastic Deformation of Silicon Electrodes in Lithium-Ion Batteries: A First-Principles Theoretical Study. *Nano Lett.* **2011**, *11*, 2962–2967.

26. Johari, P.; Qi, Y.; Shenoy, V. B. The Mixing Mechanism During Lithiation of Si Negative Electrode in Li-Ion Batteries: An *Ab Initio* Molecular Dynamics Study. *Nano Lett.* **2011**, *11*, 5494–5500.

27. Bhandakkar, T. K.; Johnson, H. T. Diffusion Induced Stresses in Buckling Battery Electrodes. *J. Mech. Phys. Solids* **2012**, *60*, 1103–1121.

28. Tang, M.; Huang, H. Y.; Meethong, N.; Kao, Y. H.; Carter, W. C.; Chiang, Y. M. Model for the Particle Size, Overpotential, and Strain Dependence of Phase Transition Pathways in Storage Electrodes: Application to Nanoscale Olivines. *Chem. Mater.* **2009**, *21*, 1557–1571.

29. Haftbaradaran, H.; Song, J.; Curtin, W. A.; Gao, H. J. Continuum and Atomistic Models of Strongly Coupled Diffusion, Stress, and Solute Concentration. *J. Power Sources* **2011**, *196*, 361–370.

30. Liu, X. H.; Huang, J. Y. *In Situ* TEM Electrochemistry of Anode Materials in Lithium Ion Batteries. *Energy Environ. Sci.* **2011**, *4*, 3844–3860.

31. Gosele, U.; Tu, K. N. Growth-Kientics of Planar Binary Diffusion Couples—Thin Film Case *versus* Bulk Cases. *J. Appl. Phys.* **1982**, *53*, 3252–3260.

32. Gosele, U.; Tu, K. N. Critical Thickness of Amorphous Phase Fromation in Binary Diffusion Couples. *J. Appl. Phys.* **1989**, *66*, 2619–2626.

33. Deal, B. E.; Grove, A. S. General Relationship for Thermal Oxidation of Silicon. *J. Appl. Phys.* **1965**, *36*, 3770–3778.

34. Shenoy, V. B.; Johari, P.; Qi, Y. Elastic Softening of Amorphous and Crystalline Li-Si Phases with Increasing Li Concentration: A First-Principles Study. *J. Power Sources* **2010**, *195*, 6825–6830.

35. Hertzberg, B.; Benson, J.; Yushin, G. *Ex-Situ* Depth-Sensing Indentation Measurements of Electrochemically Produced Si–Li Alloy Films. *Electrochem. Commun.* **2011**, *13*, 818–821.

36. Huang, S.; Fan, F.; Li, J.; Zhang, S. L.; Zhu, T. Stress Generation During Lithiation of High-Capacity Electrode Particles in Lithium Ion Batteries. *submitted* **2012**.

37. Lee, S. W.; McDowell, M. T.; Berla, L. A.; Nix, W. D.; Cui, Y. Fracture of Crystalline Silicon Nanopillars During Electrochemical Lithium Insertion. *Proc. Natl. Acad. Sci. U.S.A.* **2012**, *109*, 4080–4085.

38. Ding, N.; Xu, J.; Yao, Y. X.; Wegner, G.; Fang, X.; Chen, C. H.; Lieberwirth, I. Determination of the Diffusion Coefficient of Lithium Ions in Nano-Si. *Solid State Ionics* **2009**, *180*, 222–225.

39. Liu, X. H.; Zhang, L. Q.; Zhong, L.; Liu, Y.; Zheng, H.; Wang, J. W.; Cho, J. H.; Dayeh, S. A.; Picraux, S. T.; Sullivan, J. P.; *et al*. Ultrafast Electrochemical Lithiation of Individual Si Nanowire Anodes. *Nano Lett.* **2011**, *11*, 2251–2258.

40. Song, T.; Xia, J. L.; Lee, J. H.; Lee, D. H.; Kwon, M. S.; Choi, J. M.; Wu, J.; Doo, S. K.; Chang, H.; Il Park, W.; *et al*. Arrays of Sealed Silicon Nanotubes as Anodes for Lithium Ion Batteries. *Nano Lett.* **2010**, *10*, 1710–1716.

41. Wu, H.; Chan, G.; Choi, J. W.; Ryu, I.; Yao, Y.; McDowell, M. T.; Lee, S. W.; Jackson, A.; Yang, Y.; Hu, L. B.; *et al*. Stable Cycling of Double-Walled Silicon Nanotube Battery Anodes through Solid-Electrolyte Interphase Control. *Nat. Nanotechnol.* **2012**, *7*, 309–314.

42. Yao, Y.; McDowell, M. T.; Ryu, I.; Wu, H.; Liu, N. A.; Hu, L. B.; Nix, W. D.; Cui, Y. Interconnected Silicon Hollow Nanospheres for Lithium-Ion Battery Anodes with Long Cycle Life. *Nano Lett.* **2011**, *11*, 2949–2954.